Theory of optical transitions in Si/Ge(001) strained-layer superlattices

Mark S. Hybertsen and Michael Schlüter
AT&T Bell Laboratories, 600 Mountain Avenue, Murray Hill, New Jersey 07974
(Received 10 July 1987)

Superlattices alternating ultrathin (two, four, and six atoms) Si and Ge layers form artificial compound semiconductors. Trends and accurate transition energies for these materials are calculated based on the local-density-functional and quasiparticle self-energy approaches. The lowest transition for the Si substrate material is found to be indirect, but direct transitions to a zone-folded final state occur at slightly higher energy. The strain can be transferred to the Si layers with opposite sign by growing the superlattice on a Ge substrate. This reverses the order of the indirect and direct zone-folded transitions, which is predicted to yield an approximately direct-gap material. However, the allowed dipole matrix elements are small for these new transitions. The description of the near-band-edge states in these materials in terms of quantum wells in an effective-mass approach is found to be reasonable. In particular, both strain and confinement in the ultrathin quantum wells forming the superlattice are important. The quasiparticle energies for the particular case of the 4×4 structure have been calculated using the self-energy approach. This allows a direct comparison of the calculated transitions to recent experimental spectra for this material. In particular, the detailed features in those spectra are explained.

I. INTRODUCTION

The technique of molecular-beam epitaxy has opened many new possibilities for novel materials based on Si and Ge.[1] In particular, it has recently become possible to grow ultrathin layers of Ge on a Si substrate.[2] The Ge is perfectly bonded to the substrate resulting in a large (about 4%) built-in strain in the Ge. Alternating layers of Ge and Si with thickness of only two, four, and six atoms have been demonstrated in a superlattice extending for approximately 50 Å.[3] This structure is then capped or buffered with more Si. The superlattice region forms a quantum well in the surrounding Si. This structure may then be repeated to form multiple superlattice regions. These superlattices present a novel system with unusually thin quantum wells which may influence the optical properties. In particular, a low-energy direct optical edge might result due to the folding back of the bands of Si and Ge. This could be technologically significant because the superlattice is grown on the Si substrate and could be a contiguous part of a larger integrated device.

From a fundamental point of view, the quantum wells forming the superlattice are sufficiently narrow that band-structure techniques can be applied directly to determine the gaps and optical properties. The degree of confinement in such narrow quantum wells can be determined as well as the role of the built-in strain in the Ge layers. Some of these types of samples have been investigated using electroreflectance techniques.[3] They have revealed interesting low-energy transitions in the region of 1 eV in addition to higher-energy features. It is desirable to explain the features appearing in the spectrum. In particular, the role of zone-folded states in the low-energy transitions is of interest.

In the present study, the band structure of several Si/Ge(001) strained-layer superlattices has been investigated. For these purposes, the superlattice is periodically continued in the growth direction. Effects due to the finite number of periods can be estimated using effective-mass techniques.[4] The *ab initio* pseudopotential technique[5] together with the local-density-functional approach[6] (LDA) has been used to determine the systematic trends and band topology of the superlattices. As is well known, the minimum gap is underestimated using the LDA potential.[7] Nonetheless, the character of the gap (indirect versus direct), the dipole matrix elements for direct transitions, and trends as a function of geometry may be extracted. These calculations have been done for the 2×2 and 4×4 atomic layer superlattices lattice matched to a Si substrate. The same calculations have been performed for the case of a Ge substrated. In this case, the Ge is cubic while there is a built in strain in the Si layers (but of opposite sign).

In order to give quantitative account of the transitions in the superlattice, a full many-body calculation of the quasiparticle energies using the self-energy approach[8] has been done for the prototype case of the 4×4 superlattice. This allows direct comparison of the present calculations to recent spectroscopic experiments for this material.

The minimum gap in the Si substrate materials is indirect.[9] The conduction-band edge is made up of electrons in the transverse valleys along the Δ direction in the Brillouin zone. The longitudinal valleys are approximately folded back to the center of the superlattice Brillouin zone. These states are higher in energy due to confinement and strain effects: the compressive lateral strain places the transverse valleys below the longitudinal ones in the Ge. By growing the superlattice on a Ge

 ©1987 The American Physical Society

substrate, the Si layers are laterally expanded reversing the sign of the strain splitting. In this case, the minimum gap is predicted to be approximately direct to the zone-folded longitudinal valleys. In either case, the dipole matrix element for the direct transition to a zone-folded state at most is about 10% of that for an allowed direct transition in bulk Si or Ge. This reflects the weakness of the superlattice potential in mixing the zone-folded states with true zone-center states. In all four superlattices, the zone-folded longitudinal Δ conduction-band states are strongly confined on the Si atoms. The Γ hole states at the valence-band edge are moderately confined on the Ge atoms. This is consistent with the type-II alignment of the bands at the Si/Ge interface. One interesting result of the present work is that an effective-mass (envelope-function) theory for the energy levels near the gap region provides reasonable quantitative results in comparison to the full band structure for the 4×4 structure.

The self-energy calculations reported here allow quantitative evaluation of the optical transitions in the superlattice. Using these results, the spectra for 4×4 structure have been interpreted.[10] The lowest band edge is found to be indirect, in agreement with photocurrent measurements. All the novel features in the electroreflectance spectrum have been identified. No special self-energy effects are directly related to the confinement of some of the states in the ultrathin quantum wells forming this material.

The balance of this paper is organized as follows. The technical details of the present approach are summarized in Sec. II. The systematic trends in the bands of the superlattice materials are described in Sec. III. Section III A describes the LDA bands. The systematic effects of confinement are described in Sec. III B along with the applicability of the effective-mass picture. The results of the self-energy calculation on the 4×4 case are described in Sec. III C. Section IV is a brief conclusion.

II. SUMMARY OF PRESENT APPROACH

The preliminary step for evaluating the band structure of the superlattices is determination of the geometry. We have followed the approach of Van de Walle and Martin.[11] The transverse lattice constant $a_{\parallel}$ is fixed by the substrate, e.g., Si. Then the Si regions of the superlattice are assumed to be cubic with longitudinal lattice constant $a_{\perp}$ equal to that of the substrate $a_{\parallel}$. The Ge regions are given a longitudinal lattice constant determined by the macroscopic Poisson ratio. This leaves the interface spacing undetermined. It is fixed by taking the Si—Ge bond length to be the average of the cubic Si—Si bond length and the strained Ge—Ge bond length. The appropriate data are summarized in Table I for both the Si and Ge substrate cases. The positions of all the atoms in the (001) superlattice are now completely determined. The results of Van de Walle and Martin indicate that this is quite close to the minimum-energy geometry.[11] The (001) superlattices are periodically extended in the growth direction. The resulting material is treated in a tetragonal unit cell with four (2×2 geometry) or eight (4×4 geometry) atoms per unit cell. The symmetry group is D_{2h}. The atomic arrangement is illustrated in Fig. 1(a) for the 4×4 geometry. One should note the presence of an inversion center for these superlattices.

TABLE I. Summary of lattice constants in a.u. used to form the superlattices.

Substrate	$a_{\parallel}$	$a_{\perp\mathrm{Si}}$	$a_{\perp\mathrm{Ge}}$
Si	10.260	10.260	10.996
Ge	10.680	9.944	10.680

The band calculations are done using the *ab initio* pseudopotential[5] local-density-functional approach.[6] The pseudopotentials are taken from Bachelet, Hamann, and Schluter.[12] These include scalar-relativistic effects. The Kohn-Sham equations are solved using a plane-wave basis.[13] Plane waves up to a kinetic energy of 12 Ry are included for the systematic comparisons made in the next section. Most band energies are converged to within about 0.1 eV with respect to the size of the basis set. The only exception is the conduction-band state corresponding to the bulk $\Gamma_{2'c}$ state which requires more plane waves. For the final quasiparticle calculation reported in Sec. III C, a cutoff of 14 Ry was employed to give a better estimate of the E_0 transitions.

The LDA band energies suffer from the well-known "band-gap" problem.[7] Nonetheless, they may be used to evaluate systematic trends in the band energies as a function of the superlattice period and lattice constants. There are several reasons for this. First, the errors in the LDA band energies are well characterized for bulk Si and Ge. Full quasiparticle calculations have been done for these materials.[10] In general, the qualitative features of the LDA bands are correct. The relative energies within the valence bands and conduction bands separately are within a few tenths of an eV of the full quasiparticle energies. Also, deviations for the gap energy are about the same for Si and Ge. Second, the trends of interest are largely determined by the one-electron terms in the Hamiltonian, e.g., the degree of confinement in one region of the superlattice and the role of strain. Third, the valence-band alignment for these materials calculated within the LDA is close (within 10–15 %) to that found in a full quasiparticle calculation.[14]

In order to make a quantitative comparison to experimental spectra, however, we require the quasiparticle energies. These are determined from the electron self-energy operator,[15] Σ:

$$(T+V_{\mathrm{ext}}+V_H)\psi_{n\mathbf{k}}(\mathbf{r})+\int d\mathbf{r}'\Sigma(\mathbf{r},\mathbf{r}';E_{n\mathbf{k}}^{\mathrm{QP}})\psi_{n\mathbf{k}}(\mathbf{r}') = E_{n\mathbf{k}}^{\mathrm{QP}}\psi_{n\mathbf{k}}(\mathbf{r}) \; . \quad (1)$$

The one-electron terms correspond to the kinetic energy, electron-ion interaction, and average electrostatic interaction, respectively. All the effects of exchange and correlation are contained in the electron self-energy operator Σ. We evaluate Σ following the theory applied to bulk semiconductors and insulators previously.[8]

Briefly, the GW approximation[15] is used for Σ. This requires the full crystalline Green's function G, which is evaluated using the LDA wave functions but with a self-consistent quasiparticle spectrum. The other input required is the dynamically screened Coulomb interaction W. This is evaluated in two stages. First the full static dielectric matrices $\varepsilon_{GG'}^{-1}(\mathbf{q};\omega=0)$ are calculated using the density-functional approach (LDA) including local fields (microscopic variations in screening). The *ab initio* static dielectric matrices are then extended to finite frequency using the generalized plasmon pole model. There are no adjustable parameters. Equation (1) is then solved in first-order perturbation theory in $\Sigma - V_{xc}$ where V_{xc} is the usual exchange-correlation potential evaluated in the LDA. This procedure has proved very accurate for bulk semiconductors and insulators.[8]

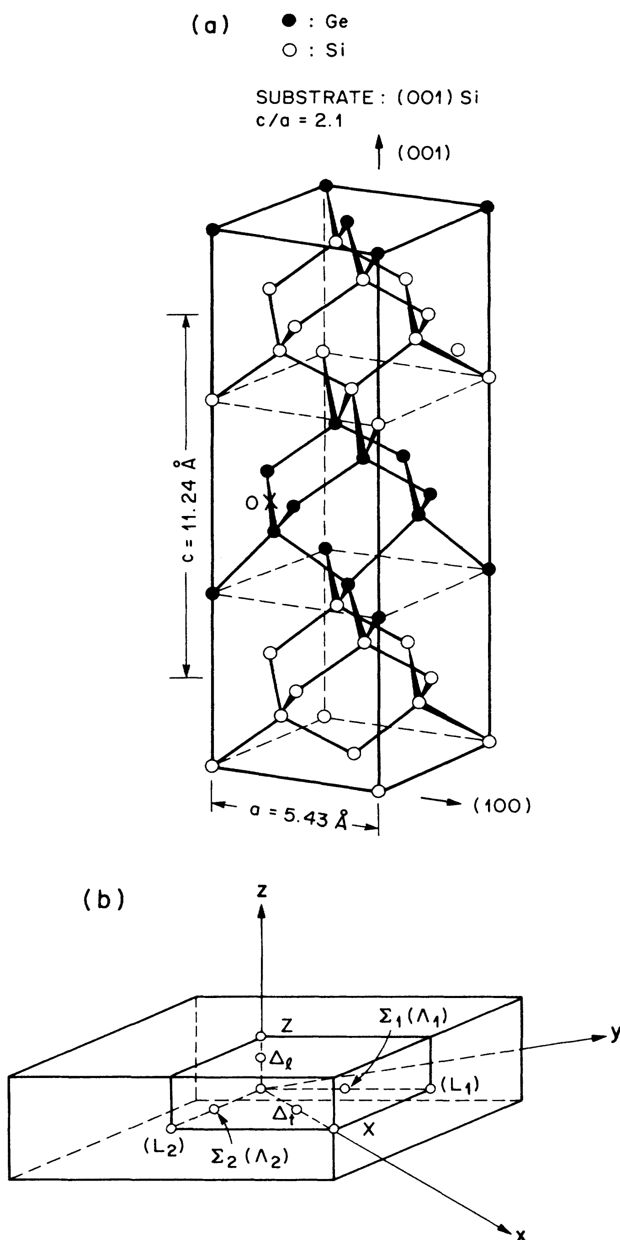

FIG. 1. The positions of the atoms in the 4×4 superlattice are shown in (a). Note that the structure is inversion symmetric about the origin indicated. One unit cell (indicated by c) contains eight layers of atoms. The corresponding Brillouin zone for the tetragonal unit cell is sketched in (b) with approximately the same orientation. Symmetry lines are indicated with notation generally taken from the underlying cubic symmetry.

We have done full quasiparticle calculations for the 4×4 superlattice matched to a Si substrate. As noted above, this involves an eight-atom tetragonal unit cell. In the calculation of the self-energy, there are several additional numerical cutoffs. The size of the dielectric matrices is determined by a momentum space cutoff: $|\mathbf{q}+\mathbf{G}|<2.5$ a.u. This results in matrices about 300×300 for each $\mathbf{q}$. Approximately 400 empty states are summed in the construction of the dielectric matrices. In the calculation of the self-energy operator, approximately 200 empty states are included and the required Brillouin-zone summation is done with nine $\mathbf{q}$ points in the irreducible wedge of the Brillouin zone including $\mathbf{q}=0$. Comparable cutoffs give results for bulk Si which agree with fully converged quasiparticle energies within 0.1 eV.

In the final comparison between the present theory and spectroscopic data, the spin-orbit interaction has been included in first-order perturbation theory. This is done by including the vector part of the *ab initio* pseudopotential[12] as described previously for bulk materials.[16] In the present context, this gives excellent results for tetragonally distorted Ge. The magnitude of the strain splittings is larger than the spin-orbit splittings.

III. RESULTS

In this section, results for the superlattices are presented. In Sec. III A, systematic trends are illustrated. Issues related to confinement in the ultrathin quantum wells forming the superlattice are discussed in Sec. III B, including the applicability of an effective-mass approach. The results for the quasiparticle energies in the 4×4 superlattice are presented in Sec. III C along with available spectroscopic data.

A. Systematic trends

The Brillouin zone corresponds to the 4×4 superlattice (an eight-atom tetragonal unit cell) is shown in Fig. 1(b). In the $k_z=0$ plane, the X point in the bulk Brillouin zone maps to the corners. The L points map to the centers of each side which also falls along Σ directions. There are two distinct Σ (or Λ) directions in the Brillouin zone because the interface bonds lift the fourfold symmetry about the growth axis. These are indicated. Along the growth direction, the X point is approximately mapped to the center of the superlattice Brillouin zone. (It is not exactly mapped to Γ because the Si and Ge longitudinal lattice constants $a_\perp$ are not equal.) In addition, points approximately half way to X map to the

center of the zone. It is precisely this zone folding that forms the basis for new direct transitions in these systems. For the 2×2 structure, the Brillouin zone is twice as large in the growth direction. Only the longitudinal Δ points near X map to Γ. The bulk L points fall in the center of the sides of the upper and lower faces instead of at $k_z=0$.

In order to have a clear picture of the zone-folded bands, the LDA bands for bulk Si and bulk Ge are shown folded back twice along the longitudinal Δ direction in Fig. 2. The bands are off-set by the calculated valence-band offset. The bands are labeled according to the appropriate symmetry designation for the diamond structure. The little group for the longitudinal Δ direction in the tetragonally distorted crystal is the same as for the Δ directions in the undistorted crystal. In Si, the Δ_1 conduction band starts from the state folded from X to Γ dispersing downwards initially. This reflects the minimum away from the X point. It intersects the Γ point a second time at around 1 eV before joining up with the Γ_{15c} state near 2.5 eV. The $\Delta_{2'}$ band disperses upwards from the state folded from X intersecting the Γ point again at about 3 eV before joining to the $\Gamma_{2'}$ state. The valence-band states are folded back in an obvious way. Turning to the Ge bands, there are two interesting points. First, the $\Gamma_{2'}$ conduction-band state is down around 0.7 eV, resulting in a rather different structure for the $\Delta_{2'}$ conduction band. Second, the valence-band-edge states are split by the tetragonal distortion into p_x,p_y states (Δ_5) and a p_z state (Δ_2).

The LDA band structure for the 4×4 structure is shown in Fig. 3 for the case of a Si substrate. The bands in Fig. 3 are shown along Δ directions: transverse to the growth direction to the bulk X point and along the growth direction up to the center of the face of the superlattice Brillouin zone. Several features of the bands are of interest. First, the usual p states forming the valence-band edge are split by the large tetragonal distortion of the Ge regions of the superlattice. The p_x,p_y states form the valence-band edge and the p_z state splits off. Second, the same distortion lifts the valley degeneracy in the Δ conduction bands. The four transverse valleys drop in energy in comparison to the two longitudinal valleys. This leads to an indirect band gap with the minimum along the transverse Δ direction about 80% of the way to the zone corner. Third, the longitudinal valleys are folded back to the region around Γ. With reference to Fig. 2, the zone-folded conduction-band states may be seen to be quite similar in structure to the Si Δ conduction bands with gaps opened at Γ and at Z. Also, in the reduced symmetry of the superlattice, the Δ_1 and $\Delta_{2'}$ bands reduce to the same representation so there are avoided crossings as well. The first pair of states is slightly split (about 0.1 eV). Following the dispersion of these states along the longitudinal Δ direction, they disperse *downwards*. This follows because the band extremum along Δ in the bulk materials does not fall at X. The dispersion is quite small because these states are strongly confined in the Si layers as discussed

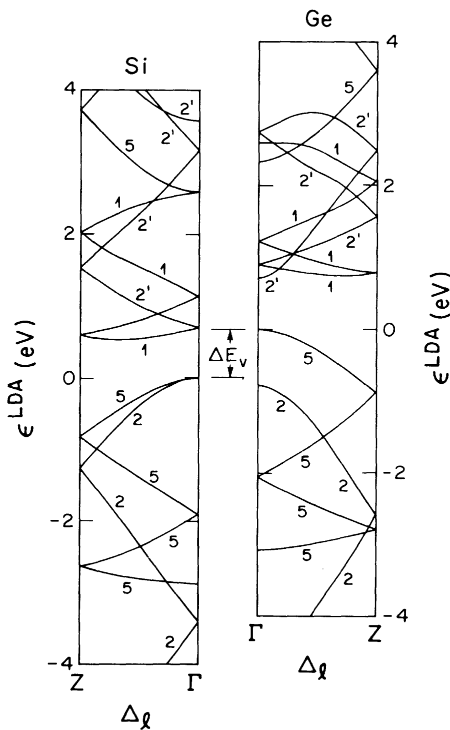

FIG. 2. The LDA bands for cubic Si and tetragonally distorted Ge are shown along the Δ direction folded back twice according to a unit cell with eight atoms analogous to the 4×4 superlattice. The bands are offset by the calculated valence-band offset between Si and lattice-matched Ge.

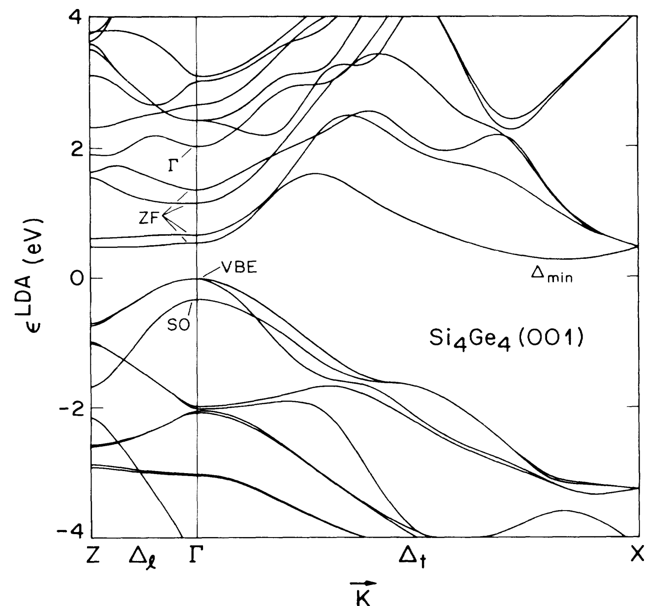

FIG. 3. The LDA band energies for the 4×4 superlattice on Si substrate plotted along the longitudinal (parallel to the growth direction) and transverse Δ directions.

in the next section. Fourth, there are a second pair of zone folded states at Γ at about 1.2 eV split by about 0.2 eV. Finally, the $\Gamma_{2'c}$ state in the superlattice falls at about 2 eV. This is approximately the average of the bulk Si and bulk Ge values.

The Δ-derived states are summarized in Table II for the Si substrate case. The strain splitting of the valence bands ($E_{x,y}-E_z$) is consistent with the large tetragonal distortion in the Ge layers and modest confinement of the holes in the Ge regions. This is further developed in the next section. The important data in Table II show that the minimum gap in each case is indirect. The gap to the zone-folded states is sufficiently larger to make this conclusion unambiguous. For the zone-folded states, we also list the calculated dipole matrix element for $\hat{x}$ polarization of the light. The units are a.u. and a "good" allowed transition would have a matrix element of order 0.5 in these units. Clearly the direct transitions derived from the zone-folded states should be relatively weak edges in absorption. The matrix elements are down by a factor of 5–20 from allowed bulk transitions. For the 4×4 structure, the superlattice potential also gives critical points at the zone face near Z. These transitions are also quite weak.

The small matrix elements are easy to understand in general terms. The folding of the states back to the zone center is not *per se* sufficient to produce a new absorption edge. In the absence of mixing with "true" Γ states of the proper symmetry, there will be *no* dipole matrix elements. The wave functions still change phase in a way characteristic of zone-edge (for example) states. The size of the matrix element is determined by the degree of mixing which in turn depends on the strength of the superlattice potential. We can estimate the relevant potential component for the 4×4 structure from the splitting of the second two zone-folded states. These derive from the Δ_1 states about half way to the zone edge in the bulk Si and Ge which are folded back to Γ. The splitting is mostly the minigap opened by the superlattice potential. This gives a potential component of order 0.1 eV. Since the relevant energy denominator is of order 1–2 eV, we immediately see that the matrix elements should be reduced by a factor of 10–20 as found above.

Table III summarizes the Δ-derived states for the Ge substrate case. Here, the strain is confined to the Si layers and, furthermore, is tensile instead of compressive. This change of sign in the strain reverses the order of the strain split Δ valleys. As a consequence, the zone-folded states are lower in energy than the transverse minima. However, the minimum gap is still not quite direct. This is due to the slight *downwards* dispersion of the zone-folded states along the growth direction. For the 4×4 structure, the dispersion is 0.12 eV, leading to a minimum LDA gap of 0.11 eV for this case. In the 2×2 structure, the initial downwards dispersion is similar, leading to a minimum about half way to the zone face for this structure. For the Ge substrate case, the dipole matrix elements shown are for z polarization of the light. This choice is made because the reversal of the strain has reversed the character of the valence-band-edge states. The highest state is now of p_z character. The matrix elements follow the same pattern as for the Si substrate case. In particular, the lowest zone-folded state does not connect to the valence-band edge via an allowed transition for the 4×4 case. The direct absorption edge is to the second state. In the 2×2 structure, the lowest zone-folded state is weakly allowed, but the minimum gap is still indirect.

There is also interesting structure in the higher-energy direct transitions. The transition energies at the Γ point and the mapped L point are indicated in Table IV. We restrict ourselves to the lower-energy transitions (generally below the direct absorption edge in Si). The E_0 transition is taken to be from the valence-band-edge complex (including the strain split-off states) to the s state corresponding to the $\Gamma_{2'c}$ states in the bulk materials. These light mass states generally fall at an average energy between the Si and Ge cases, although some confinement in the Ge region is discernible. The L-point

TABLE II. The LDA band energies for the Δ states for the two-monolayer and four-monolayer superlattices on a Si substrate: transverse minimum ($\Delta^t_{\min}$), longitudinal states folded back to the zone center (ZF). Also shown is the strain splitting of the valence-band-edge states ($E_{x,y}-E_z$). Energies are in eV relative to the valence-band edge. For the direct transitions, the dipole matrix elements connecting to the valence-band-edge states are given in a.u.

Si substrate	2×2	4×4
$E_{x,y}-E_z$	0.34	0.32
$\Delta^t_{\min}$	0.20	0.29
ZF	0.68	0.55
($\langle v\|p_x\|c\rangle$)	(0.125)	(0.0)
	0.86	0.66
	(0.0)	(−0.025)
		1.16
		(−0.079)
		1.36
		(0.0)

TABLE III. Same as Table II but for the Ge substrate case.

Ge substrate	2×2	4×4
$E_z-E_{x,y}$	0.15	0.21
$\Delta^t_{\min}$	0.49	0.55
ZF	0.43	0.23
($\langle v\|p_z\|c\rangle$)	(−0.044)	(0.0)
	0.61	0.33
	(0.0)	(−0.033)
		0.76
		(−0.054)
		0.93
		(0.0)

TABLE IV. Direct transitions in the superlattices at the Γ and mapped L points of the new Brillouin zone.

	Si substrate		Ge substrate	
	2×2	4×4	2×2	4×4
E_0	2.16	2.01	1.89	1.78
$(\Gamma\rightarrow\Gamma)$	2.50	2.33	2.04	1.99
E_1	1.36	1.85, 1.89	1.54–1.60	1.92–2.01
$(L\rightarrow L)$	1.98, 2.01	2.16	1.96	2.23
	2.16	2.47–2.51	2.25–2.35	2.58, 2.60
	2.50		2.87	
	2.96–3.05			

(including some Σ bands in the 4×4 structure) transitions exhibit a much richer structure. This is attributable to two factors. First, the strain splitting of the bulk $L_{3'v}$ states is of order 0.5 eV in this instance. Second, as noted above, the interface bond orientation distinguishes two distinct Λ directions which are otherwise equivalent in the bulk materials.

B. Role of confinement and an effective-mass picture

Despite the ultrathin quantum wells forming the superlattice, confinement of some states is quite striking. For the 4×4 superlattice on a Si substrate, this is illustrated in Fig. 4. Perspective plots of $|\psi(\mathbf{r})|^2$ are shown for $\mathbf{r}$ in the $(\bar{1}01)$ plane that approximately contains a chain of bonds running through the structure. (The bond chain would be exactly in this plane if the Ge regions were cubic.) The figures show a sequence of bonds passing through four Si atoms, four Ge atoms, and finally four more Si atoms. Figure 4(a) shows the valence-band-edge states. These are seen to be weakly confined in the Ge regions. The second zone-folded state at Γ (with allowed dipole matrix elements) is plotted in Fig. 4(b). This state is strongly confined to the Si regions of the superlattice. The microscopic structure of the wave function is characteristic of X_{1c} states in bulk Si. Finally, the transverse X_{1c} states are shown in Fig. 4(c). These are clearly unconfined and are of X_{1c} character in both the Si and Ge regions.

The integrated weight in the Si region of the superlattices of several states are tabulated in Table V for the cases considered here. In general, the spin-orbit splitting together with the strain produces three distinct hole bands near the valence-band edge. These are listed in Table V with H_1 being the highest. Consider first the Si substrate case. The H_1 is the most confined valence-band-edge state, being about 60% in the Ge region for the 4×4 geometry. The zone-folded state listed is the first one with nonzero dipole matrix elements to the valence-band edge. In the 4×4 structure, this is strongly confined to the Si region, as illustrated in Fig. 4(b). Finally, the transverse minima are unconfined. These are systematic differences between the 4×4 case and the 2×2 case. The states in the narrower wells generally exhibit considerably less confinement. The only truly confined states are the lowest pair of zone-folded states at Γ in the 4×4 structure.

These results can be understood in terms of an effective-mass picture. The envelope approximation is made in each portion of the superlattice and the potential change across the interface is modeled as abrupt.[4,17] The result is a square-wave type of potential which is to

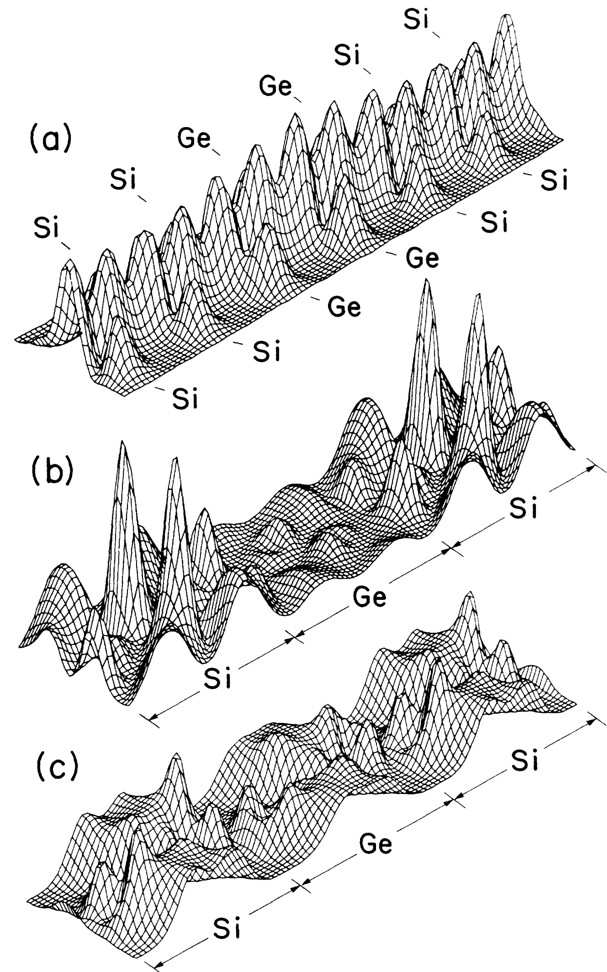

FIG. 4. The $|\psi(\mathbf{r})|^2$ is plotted in a plane with the bond chain passing through both the Si and Ge regions of the 4×4 superlattice for the following: (a) valence-band-edge states; (b) zone-folded conduction-band state; (c) transverse X_{1c} conduction-band states.

TABLE V. The integrated weight of $|\psi(\mathbf{r})|^2$ in the Si region of the superlattice.

w_{Si}	Si substrate 2×2	Si substrate 4×4	Ge substrate 2×2	Ge substrate 4×4
H_3	0.56	0.54	0.48	0.51
H_2	0.48	0.48	0.44	0.42
H_1	0.44	0.41	0.61	0.56
ZF	0.57	0.78	0.55	0.80
$\Delta_{\min}$	0.60	0.54	0.66	0.55

be used in an effective-mass approach with boundary conditions ensuring continuity of the envelope function and the current. Using the LDA results for the valence-band-edge alignment, band gaps, and spin-orbit and strain splittings, the appropriate potentials can be constructed. This is done for the valence-band-edge complex and X_{1c}-derived conduction-band states in Fig. 5. The valence-band-edge states are indexed by m_J, the magnetic quantum number for total angular momentum. It is clear from the diagram [Fig. 5(b)] that the hole states will be modestly confined in the Ge regions with the highest state being most confined. The degree of confinement is small because the hole masses in the constituent materials are quite light (of order 0.2 or less depending on band). The barrier for the X_{1c}-derived conduction bands depends on orientation due to the strain in the Ge regions [Fig. 5(a)]. The longitudinal valleys see a large barrier. In addition, the longitudinal conduction-band mass is large (of order 1) so confinement is strong. However, the transverse valleys see a considerably smaller barrier. Together with the small transverse mass (of order 0.2), there is essentially no confinement. The trends illustrated in Table V are in qualitative agreement with this picture. The smaller degree of confinement in the 2×2 geometry is consistent with the thinner wells.

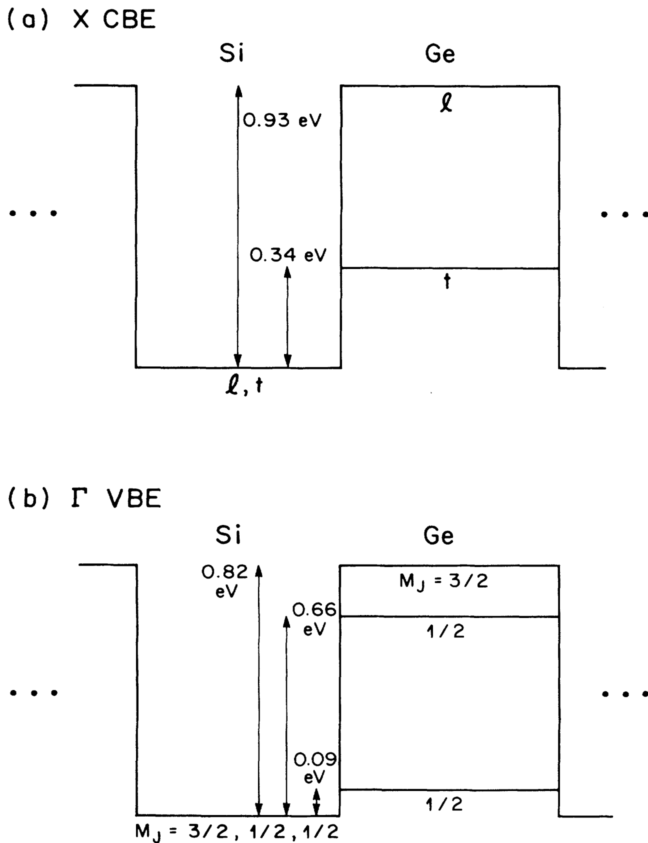

FIG. 5. The appropriate barriers for Si substrate superlattices alternating cubic Si and strained Ge for (a) conduction-band-edge states and (b) valence-band-edge states in an effective-mass picture.

Surprisingly, the effective-mass picture is already quite reasonable quantitatively for the 4×4 structure. This is illustrated in Table VI. The effective-mass equations have been solved using the barriers given in Fig. 5 and band masses derived from the LDA band structure of cubic Si and tetragonally distorted Ge (including the spin-orbit interaction). The results are compared to the full LDA calculation both for the transition energies and the degree of confinement. The overall agreement is quite good. The effective-mass results are within a few hundredths of an eV for most cases. The only feature not reproduced is the splitting of the zone-folded conduction-band states. This, however, is attributable to the microscopic structure of the superlattice; the Ge and Si regions are not commensurate due to the strain, a feature not taken into account in the effective-mass picture.

Turning now to the Ge substrate case, there are two interesting differences. First, the character of the hole states is quite different. The strain has been transferred to the Si regions and has the opposite sign. Essentially, the p_z states are split up instead of down. This was reflected in the matrix elements discussed in the preceding section. Here, we also find that the valence-band edge is essentially unconfined, with somewhat more weight in the Si regions. In the 4×4 structure, the state H_2 is the one which is more confined in the Ge regions analogous to the valence-band edge in the Si substrate case above. This can be understood with reference to the quantum-well potentials shown in Fig. 6. The hole states in the Si region are split by strain. (The spin-orbit splitting is neglected.) In the Ge region they are spin-orbit split. The highest hole state will be $m_J=\frac{1}{2}$ which is confined by a small barrier. The $m_J=\frac{3}{2}$ state is confined by the largest barrier and corresponds to the H_2 state modestly confined in the Ge regions. Finally, the H_3 state is essentially unconfined. The trend from the 4×4 to 2×2 structure is not entirely consistent with less confinement in thinner quantum wells, suggesting that the microscopic potential at the interface is more important in that case. Also, for the $m_J=\frac{1}{2}$ states, neglect of interband coupling in an envelope approximation breaks down.

The other important change in the Ge substrate case is the reversal of the order of the conduction-band valleys. Here, the longitudinal valley is lower. This is shown in Fig. 6(a). The change in strain together with

TABLE VI. The microscopic LDA band energies (transitions) are compared to the results of the effective-mass approach. The integrated weight of $|\psi(\mathbf{r})|^2$ in the Si region of the superlattice is also compared.

	LDA		EM	
	E	$\langle w_{\rm Si}\rangle$	E	$\langle w_{\rm Si}\rangle$
H_3	−0.42	0.54	−0.39	0.48
H_2	−0.10	0.48	−0.09	0.45
H_1	0.00	0.41	0.00	0.43
ZF	0.49	0.84	0.61	0.73
	0.60	0.78		
E_0	1.96	0.38	1.94	0.39
$\Delta_{\rm min}$	0.23	0.54	0.25	0.51

the confinement of the zone-folded states leads to a nearly direct gap. That the zone-folded states disperse downwards is a detail of the band structure which is outside the scope of the effective-mass picture.

C. Quasiparticle energies in Si_4Ge_4(001)

The calculated quasiparticle energies for the superlattice can be compared to the LDA eigenvalues discussed above. This gives us a way of assessing the reliability of the trends identified using the LDA bands as well as pointing out any novel self-energy effects in this superlattice. The difference $E^{\rm QP}-\varepsilon^{\rm LDA}$ is plotted as a function of $E^{\rm QP}$ in Fig. 7 for the superlattice as well as bulk Si and tetragonally distorted Ge. The three sets of data are aligned at the valence-band edge. Generally, the self-energy corrections so defined fall on smooth lines for the conduction-band and valence-band states separately. This is exactly what was found for bulk semiconductors.[8] Closer examination of the data does reveal some systematic changes. These are attributable to corrections to the valence-band alignment and the bulk deformation potentials. The quasiparticle calculation yields noticeably different values for these quantities as will be discussed elsewhere.[14,18] Otherwise, the qualitative features of the self-energy results for the superlattice are the same as for bulk materials. In particular, confinement of some states to either Si or Ge regions does not play a quantitatively important role in the self-energy operator in comparison to the LDA potential. This is not too surprising since the corrections arising from self-energy effects in bulk Si and bulk Ge are quite similar.

The results of the present quasiparticle calculation have been used to interpret the experimental spectra for the 4×4 superlattice. Results of the present self-energy approach give transition energies in excellent agreement with experiment for both bulk Si and bulk Ge.[8] We can therefore be confident in our assessments of the magnitudes of the transition energies involved.

The most basic feature of the 4×4 superlattice is the indirect gap. The calculation gives an indirect gap of 0.85 eV. A second indirect edge due to the light holes is calculated to enter at 0.95 eV. This is in excellent agreement with the absorption edge measured in photocurrent.[10] The photoresponse as a function of photon energy clearly does not fit the usual $(E-E_0)^{1/2}$ behavior for an allowed direct edge. It is fit quite well by two indirect edges at 0.78 and 0.90 eV, in excellent agreement with the theory both in magnitude and in splitting. One should note that a phonon-assisted process for the in-

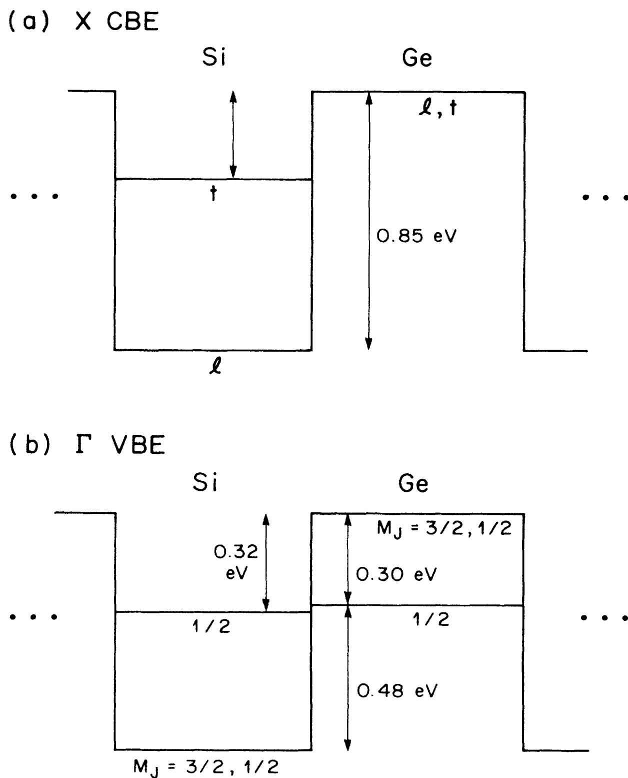

FIG. 6. The appropriate barriers for Ge substrate superlattices alternating strained Si and cubic Ge for (a) conduction-band-edge states and (b) valence-band-edge states in an effective-mass picture.

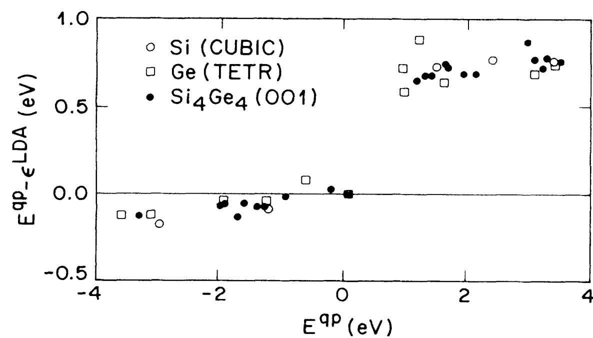

FIG. 7. The calculated difference $E^{\rm QP}-\varepsilon^{\rm LDA}$ is plotted against the quasiparticle energy $E^{\rm QP}$ for the 4×4 superlattice as well as cubic Si and tetragonally distorted Ge. All values are taken with respect to that at the valence-band edge.

direct absorption will be dominated by phonon emission for the present case so that the actual electronic energy gap may be smaller by the phonon energy (of order 0.03–0.05 eV). Other aspects of the sample structure also affect the exact magnitude and interpretation of the minimum absorption energy, as discussed in Sec. IV below.

Extensive electroreflectance (ER) measurements have been made on the 4×4 superlattice grown as described in the Introduction.[3,10] The measurements have been done for two different samples grown independently. The resulting spectra show a rich variety of features below the energy of the bulk Si E_1 transition (3.4 eV). The transitions responsible for this structure must be characteristic of the superlattice region of the sample in some way. The spectra for the two samples are in general agreement. The line shape in the infrared region of the spectrum differs. Also, a strong feature near 1.8 eV appears for only one sample, although a shoulder in the same spectral region can be discerned in the spectrum for the other sample. Finally, the higher-energy structure appears shifted in energy by about 0.1 eV between spectra for the two samples. In order to determine the experimental critical-point energies as well as linewidths, the spectra are fit to a generalized line-shape function. With closely spaced features, precise extraction of the critical-point energy remains somewhat uncertain. The best-fit values for both samples are indicated in Table VII. The data differ by about 0.1 eV, at most, giving a rough measure of the error bars on the measured critical points due to sample variation, differences in measurement conditions, and fitting uncertainties. This uncertainty is comparable to the precision expected for the calculated quasiparticle energies (0.1 eV).

A reproducible feature is observed near 0.8 eV. Based on the present calculation, we have to assign this feature to the indirect absorption edge. The second feature in the ER spectra at 1.1–1.25 eV is assigned to the *first* transition to a zone-folded state. This is different from the interpretation put forward by other groups.[19] However, it is the only interpretation consistent both with the accuracy of the quasiparticle calculation and the photocurrent measurements. The intensity expected from the matrix elements in Table II is in fact comparable to that from an indirect edge, at least on the basis of the matrix elements for the phonon-assisted process.[20] These features are quite comparable in the ER spectra. A third feature has been observed on one sample around 1.8 eV.[10] This is assigned to the second allowed transition to a zone-folded state. All of these features are predicted to occur as doublets, although this is not clearly resolved in the spectra. Transitions from the split-off hole band do not play an important role because the light in the experiment is polarized in the x-y plane (transverse to the growth direction). These results are summarized in Table VII.

TABLE VII. The transition energies calculated from the quasiparticle (QP) band structure of the extended 4×4 superlattice are compared to the features observed in electroreflectance (ER) for two distinct samples (each value respectively forming the range indicated) and photocurrent (PC) experiments.

	QP	ER[a]	PC[b]
E_g	0.85, 0.95	0.76–0.76	0.78, 0.90
ZF	1.24, 1.34	1.1–1.25	
	1.76, 1.86	1.8	
E_0	2.4, 2.5	2.2–2.3	
E_1	2.50, 2.55	2.45–2.58	
	2.88	2.65–2.81	
	3.18, 3.20	2.95–3.06	
	3.24, 3.28		

[a]References 3 and 10.
[b]Reference 10.

The other features of the ER spectrum can be interpreted in terms of standard transitions in Si and Ge modified by the superlattice geometry. These are all dipole-allowed transitions. The 2.2–2.3-eV feature corresponds to the E_0 transition at the zone center. Only transitions from the heavy- and light-hole bands contribute due to the polarization of the light. Transitions from the split-off valence band are quite weak due to its strong p_z character. One should note that the experiment is done at room temperature while the theory predicts $T=0$ gaps. The E_0 feature will move up about 0.1 eV as the temperature is lowered to zero. Another important point is that both the electrons and the holes are confined in the superlattice region of the sample (about 50 Å). This adds about 0.1 eV to the theoretical value for the transition energy.

The rest of the features are attributed to modified E_1 transitions. In bulk Si and Ge, these arise from direct transitions at the L point in the Brillouin zone or along Λ. In general, the energy of the critical point is quite close to the transition energy at the L point. Both the strain and the spin-orbit interaction split the bulk valence-band state at L into two components. This leads to the standard E_1 and $E_1+\Delta_1$ features in the spectrum. This persists also in the alloy spectrum. For the superlattice, there is an additional splitting due to the inequivalent Λ (Σ) directions parallel and perpendicular to the interface bonds. This leads to further distinct transition energies at the mapped L point of the superlattice Brillouin zone as discussed in Sec. III A. The dipole-allowed transitions are compared to the features in the ER spectrum in Table VII. The correspondence is excellent, supporting the assignment of these features as E_1-derived transitions.

IV. CONCLUSIONS AND DISCUSSION

We have analyzed the band structure of extended superlattices formed by alternating a few monolayers of Si and Ge. The effects of strain and confinement play an important role in determining the character of the absorption edge as well as higher-energy structure in optical spectra. In particular, for superlattices grown on a Si substrate (cubic Si alternating with strained Ge), the

minimum gap is indirect to states along the transverse Δ directions near X. Zone-folded states coming from the longitudinal Δ directions lie higher in energy and have weak dipole matrix elements coupling to the valence-band-edge states. Alternatively, growing the superlattice on a Ge substrate (strained Si alternating with cubic Ge) leads to an approximately direct-gap semiconductor. This is due to the reversal of the sign of the strain splitting of the conduction-band minima along Δ. These superlattices are in fact still indirect due to the slight downwards dispersion of the zone-folded states away from the zone center. This difference is not too much larger than the phonon energies that would be involved in phonon-assisted transitions. We also note that the finite (small) number of superlattice periods in actual samples will break down **k** conservation along the growth direction, rendering this small degree of indirectness irrelevant.

The quasiparticle energies for the 4×4 superlattice have been calculated using the self-energy approach. This has allowed quantitative interpretation of the photocurrent and electroreflectance data for this material. The indirect character of the absorption edge is identified. All the features in the spectra are identified.

Several open questions remain. The observation of an indirect edge in electroreflectance, although not unique, is unusual. The indirect and zone-folded features in the spectra have an intensity comparable to each other and also to the dipole-allowed transitions observed. Similarly, the two indirect components observed in the photocurrent data have an intensity ratio that is not explainable strictly on the basis of the extended superlattice states. One can estimate the expected ratio of absorption due to the light- and heavy-hole bands in the extended superlattice from the masses and the strain and spin-orbit mixing of those p states. The result is that these cross sections are at most comparable and the heavy-hole absorption is probably larger. The photocurrent signals are the opposite with the light-hole component larger by about a factor of 3.

The one aspect of these new materials *as grown* that has not been taken explicitly into account is the finite number of superlattice periods. Essentially, the superlattice forms a quantum-well region in a Si matrix. Viewed in this way, and with reference to Fig. 5, the holes are confined in the superlattice region, but the electrons at the conduction-band minima are not. In fact, the electrons should be in the Si region with a barrier formed by the superlattice region. These features have minimal impact on the quantitative levels in the superlattice region. Shifts in energy due to confinement in the 50-Å quantum well are of order or smaller than the estimated uncertainty in the quasiparticle transition energies (of order 0.1 eV). However, this aspect of the problem may well have consequences for the intensity of the features observed in the experimental spectra.

The role of confinement in the superlattice region was mentioned in Sec. III C for the E_0 transitions where both electrons and holes are confined. For the lowest transition, several points can be made. First, the heavy holes are in a quantum well about 0.5 eV deep. The corresponding confinement energy is about 0.05 eV. The light holes are in a well about 0.4 eV deep and have a similar confinement energy. This increases the calculated indirect gap. It also affects the external quantum efficiency in the photocurrent measurements where the signal is due to collection of the photoelectrons and photoholes. The holes must escape from the superlattice region of the sample in the electric field applied for collecting the photocurrent. Clearly the light holes, being in a shallower well, escape more easily and hence contribute more to the photocurrent signal. Second, the superlattice conduction-band edge falls about 0.1 eV above the bulk Si conduction-band edge. As a consequence, the electrons are not confined to the superlattice region. Further, one might speculate that the absorption creates electrons in the bulk Si states which penetrate into the superlattice region. This would reduce the calculated minimum gap by about 0.1 eV. Also, since the **k** conservation along the growth direction is thus broken, the label "indirect" may be somewhat of a misnomer in this case.

Clearly, the net effect of the finite superlattice extent on the calculated minimum gap energy is quite small. However, the role which the sample geometry plays in the actual absorption intensity and energy dependence may be more important. One may also propose other mechanisms for indirect absorption, including steps at the growth interfaces or defects. Both could take up the necessary momentum. This remains an outstanding problem which requires further work.

ACKNOWLEDGMENTS

It is a pleasure to acknowledge many interesting discussions with D. V. Lang, T. Pearsall, J. Bevk, and F. H. Pollack on experimental aspects of these superlattice systems, and with R. People and S. A. Jackson on the effective-mass approach to the superlattice energies.

[1]J. C. Bean, L. C. Feldman, A. T. Fiory, S. Nakahara, and I. K. Robinson, J. Vac. Sci. Technol. A **2**, 436 (1984).
[2]J. Bevk, J. P. Mannaerts, L. C. Feldman, B. A. Davidson, and A. Ourmazd, Appl. Phys. Lett. **49**, 286 (1986).
[3]T. P. Pearsall, J. Bevk, L. C. Feldman, J. M. Bonar, J. P. Mannaerts, and A. Oarmazd, Phys. Rev. Lett. **58**, 729 (1987); J. Bevk, A. Ourmazd, L. C. Feldman, T. P. Pearsall, J. M. Bonar, B. A. Davidson, and J. P. Mannaerts, Appl. Phys. Lett. **50**, 760 (1987).
[4]G. Bastard, Phys. Rev. B **24**, 5693 (1981).
[5]D. R. Hamann, M. Schlüter, and C. Chiang, Phys. Rev. Lett. **43**, 1494 (1979).
[6]P. Hohenberg and W. Kohn, Phys. Rev. **136**, B864 (1964); W. Kohn and L. J. Sham, *ibid.* **140**, A1133 (1965). The electron gas data used is taken from D. M. Ceperley and B. I. Alder, Phys. Rev. Lett. **45**, 566 (1980) as parametrized in J. P. Per-

dew and A. Zunger, Phys. Rev. B **23**, 5048 (1981).

[7]D. R. Hamann, Phys. Rev. Lett. **42**, 662 (1979); L. J. Sham and M. Schlüter, *ibid.* **51**, 1888 (1983).

[8]M. S. Hybertsen and S. G. Louie, Phys. Rev. Lett. **55**, 1418 (1985); Phys. Rev. B **34**, 5390 (1986); R. W. Godby, M. Schlüter, and L. J. Sham, Phys. Rev. Lett. **56**, 2415 (1986); Phys. Rev. B **35**, 4170 (1987).

[9]The indirect gap in this case has already been noted in another context: S. Ciraci and I. P. Batra, Phys. Rev. Lett. **58**, 2114 (1987).

[10]M. S. Hybertsen, M. Schlüter, R. People, S. A. Jackson, D. V. Lang, T. P. Pearsall, J. M. Vandenberg, J. C. Bean, and J. Bevk (unpublished).

[11]C. G. Van de Walle and R. M. Martin, Phys. Rev. B **34**, 5621 (1986).

[12]G. B. Bachelet, D. R. Hamann, and M. Schlüter, Phys. Rev. B **26**, 4199 (1982).

[13]J. Ihm, A. Zunger, and M. L. Cohen, J. Phys. C **12**, 4409 (1979).

[14]M. S. Hybertsen and M. Schlüter (unpublished).

[15]L. Hedin and S. Lundqvist, in *Solid State Physics,* edited by H. Ehrenreich, F. Seitz, and D. Turnbull (Academic, New York, 1969), Vol. 23, p. 1.

[16]M. S. Hybertsen and S. G. Louie, Phys. Rev. B **34**, 2920 (1986).

[17]R. People and S. A. Jackson, Phys. Rev. B **36**, 1310 (1987).

[18]The correction to the valence-band alignment is about 10–15% for this system. This is a technically important point because it implies that the degree of confinement of the wave function as calculated in the LDA is approximately correct. In the present approach, the new quasiparticle wave function in Eq. (1) is not calculated. Rather, the quasiparticle energy is obtained from the first-order corrections $\langle n\mathbf{k} | \Sigma - V_{xc} | n\mathbf{k} \rangle$.

[19]S. Froyen, D. M. Wood, and A. Zunger, Phys. Rev. B **36**, 4547 (1987). The ER spectrum is not explicitly interpreted in this paper. However, a recent calculation based on a tight-binding approach interprets the two lowest features in the ER as due to transitions to zone-folded levels, in contrast to the present interpretation: Phys. Rev. Lett. **59**, 1022 (1987).

[20]The electron and hole phonon matrix elements are known for the bulk materials from O. J. Glembocki and F. H. Pollack, Phys. Rev. Lett. **48**, 413 (1982); Phys. Rev. B **25**, 1193 (1982). These can be combined with the calculated dipole matrix elements for direct transitions to obtain the second-order matrix elements appearing in the phonon-assisted indirect process.